Dyes and Pigments 208 (2022) 110818

Contents lists available at ScienceDirect

Dyes and Pigments

journal homepage: www.elsevier.com/locate/dyepig

Boosting the efficiency of organic solar cells via plasmonic gold nanoparticles and thiol functionalized conjugated polymer

Oguzhan Karakurt [a], Eda Alemdar [a], Mert Can Erer [a], Duygu Cevher [b], Selin Gulmez [a], Umut Taylan [c], Sevki Can Cevher [d], Gonul Hizalan Ozsoy [e,**], Bulend Ortac [c], Ali Cirpan [a,b,e,f,*]

[a] Department of Chemistry, Middle East Technical University (METU), 06800, Ankara, Turkey
[b] Department of Polymer Science and Technology, Middle East Technical University, 06800, Ankara, Turkey
[c] UNAM — National Nanotechnology Research Center and Institute of Materials Science and Nanotechnology, Bilkent University, 06800, Ankara, Turkey
[d] Department of Engineering Fundamental Sciences, Sivas University of Science and Technology, Sivas, 58070, Turkey
[e] ODTU GUNAM, Middle East Technical University, 06800, Ankara, Turkey
[f] Department of Micro and Nanotechnology, Middle East Technical University, Ankara, 06800, Turkey

ARTICLE INFO

Keywords:
Gold nanoparticles
Surface plasmon
Bulk heterojunction
Organic solar cell
Thiol-gold interaction

ABSTRACT

Conjugated polymers are promising low-cost, lightweight, and flexible candidates for scalable photovoltaic applications to establish decarbonized energy technologies. However, they possess deficiencies in terms of their lower charge mobility and exciton diffusion length compared to their inorganic counterparts, impeding the efficient charge extraction at high active layer thickness values. In this manner, active layer composition should be tuned to improve light harvesting enabling efficient charge transport. This work presents two new approaches to achieve higher photovoltaic performance for organic photovoltaic systems; thiol modification of the polymers for improved morphological features, and incorporation of ligand-free gold nanoparticles with surface plasmon absorption into the active layer to be stabilized by the covalent interaction with the thiol side groups of the polymers. To achieve this goal, a benzoxadiazole bearing polymer (**POxT**) and its bromine (**POxT-Br**) and thiol (**POxT-SH**) comprising derivatives were synthesized, their electrochemical, optical, photovoltaic, and morphological characterizations were performed. For photovoltaic characterizations, conventional device architecture of ITO/PEDOT:PSS/polymer:$PC_{71}BM$/LiF/Al was utilized, where the **POxT-SH** showed the highest J_{SC} and PCE values, 6.52 mA/cm^2 and 2.71%, respectively. Gold nanoparticles were synthesized via laser ablation method, and upon incorporation, the PCE value was boosted to 3.29%, with an increase of 21.4% compared to **POxT-SH** comprising organic solar cells.

1. Introduction

Rapid increase in global warming necessitates the transformation of global energy systems to renewable sources. In this manner, photovoltaic technologies are expected to provide the next-generation clean energy production technologies to replace the depleting sources of fossil fuels, aiming the mitigation of climate change by reducing the greenhouse gas emission. Conjugated polymers offer several advantages for photovoltaic systems via their low cost, light weight, flexibility, use in roll-to-roll production, and environmentally benign nature compared to their inorganic counterparts [1–4]. Attention on polymer solar cells composed of active layers based on conjugated polymer: fullerene/non fullerene blends, namely the bulk heterojunction (BHJ) organic solar cells (OSCs) is paid. This is due to the enhanced charge extraction and reduced exciton recombination, via increased donor-acceptor interfacial area shortened distance for excitons to travel for charge separation [5–7]. However, conjugated polymers possess low charge mobilities and short diffusion lengths which limits the active layer thickness. There is a tradeoff between photogenerated carrier collection and light absorption. Therefore, development of active layers with reduced thickness and

* Corresponding author. Department of Chemistry, Middle East Technical University (METU), 06800, Ankara, Turkey.
** Corresponding author. ODTU - GUNAM, Middle East Technical University, 06800, Ankara, Turkey.
E-mail addresses: karakurt@metu.edu.tr, oguzhankarakurt12@gmail.com (O. Karakurt), ealemdar@metu.edu.tr (E. Alemdar), mertcanerer@gmail.com (M.C. Erer), duygucevher09@gmail.com (D. Cevher), selingulmez1996@gmail.com (S. Gulmez), umut.taylan@bilkent.edu.tr (U. Taylan), cevhersc@gmail.com (S.C. Cevher), gonul.ozsoy@odtugunam.org (G. Hizalan Ozsoy), ortac@unam.bilkent.edu.tr (B. Ortac), acirpan@metu.edu.tr, aacirpan@gmail.com (A. Cirpan).

https://doi.org/10.1016/j.dyepig.2022.110818
Received 15 August 2022; Received in revised form 30 September 2022; Accepted 30 September 2022
Available online 13 October 2022

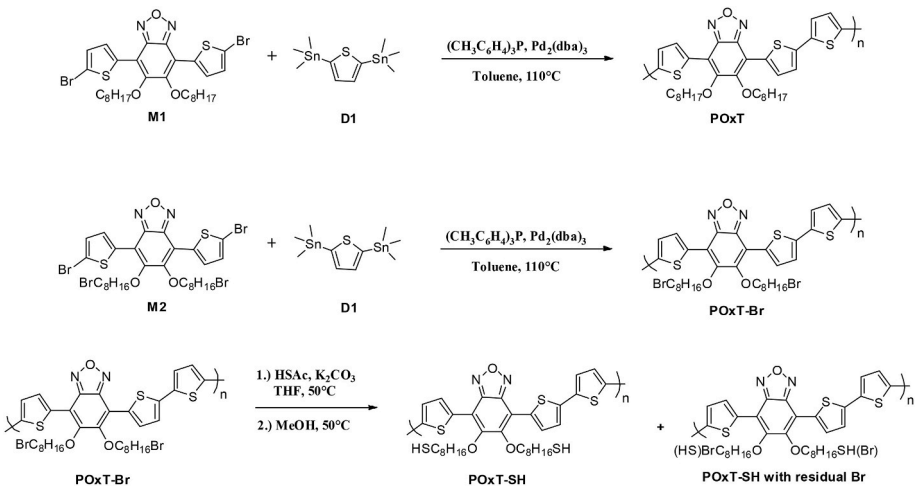

Scheme 1. Synthetic route for the polymers.

improved light harvesting ability is an efficient approach to increase the photocurrent values for OSCs [8,9]. Incorporation of periodic nanostructures [10] fabrication of diffraction gratings [11] and inclusion of metallic nanoparticles are the proposed methods to enhance light trapping in photovoltaics. Among these methods inclusion of metal nanoparticles comes into prominence with its ease of incorporation.

Metallic nanoparticles can be incorporated in organic solar cells with different design strategies depending on the site where nanoparticles are embedded. In literature, plasmonic effect of nanoparticles on ITO [12], in PEDOT:PSS layer [13–17], in PANI layer [18], in ZnO buffer layer [19], in MoO_x buffer layer [20], in active layer [21–23] and in between the hole transport and active layer [24,25] were investigated.

Inclusion of metal nanoparticles (NPs) in the active layer is an efficient strategy to enhance the light-harvesting capability within a range of wavelengths. Metal NPs have unique localized surface plasmon resonance (LSPR) properties which augments the light absorption and scattering inside the active layer, depending on size, shape and concentration of NPs. Kim and Carroll have reported that the direct addition of Gold (Au) or Silver (Ag) nanoparticles to the active layer solutions also results in films having higher electrical conductivity and lower series resistance via the introduction of the dopant states [9,26,27]. In this regard, metallic NP introduction is proven to assist the active layer to achieve enhanced photocurrent production at reduced thickness values, suppressing the charge recombination in between.

In various studies metallic NPs have been successfully embedded in active layers of OSCs in which nanoparticles were randomly distributed. However, in this case aggregation of NPs which disrupts the active layer morphology, is inevitable. To the best of our knowledge, no scientific work has been reported to control the distribution of NPs inside the active layer of BHJ solar cells. This work proposes a versatile and effective strategy for performance improvement of OSCs through incorporation AuNPs in the active layer with controlled distribution by using thiol-modified conjugated polymers. The covalent bonding between gold and sulfur provides a strong but tunable interaction, which is crucial for nanostructure stabilization and electronic interactions between gold NPs and thiol end-functionalized polymeric ligands. Such interaction is widely utilized in distinct research fields such as molecular biology, material science, and inorganic chemistry [28–33]. The sulfur-gold nanoparticle (AuNPs) interaction is proven to be sufficient to construct a covalent bonding that provides controlled distribution of AuNPs in the active layer. Hence, the use of thiol modified polymers as the electron donor molecules with AuNPs yields a controlled morphology where the polymers are aligned upon interaction with the NPs, with improved charge transport properties.

This work reveals that several benefits arose from using AuNPs in the active layer of an OSC and controlling their distribution by using thiol-modified conjugated polymers. To investigate the effect of thiol modification on the nanoparticle distribution and overall device performance, three alternating conjugated copolymers with varying chains of alkyl, **POxT**, **POxT-Br**, and **POxT-SH** (Scheme 1) were synthesized. The synthesis and characterization of these polymers and the effect of thiol modification and AuNPs addition on photovoltaic properties of these polymers will be discussed.

2. Results and discussion

2.1. Synthesis and characterization

Synthetic pathways of monomers **M1** and **M2** are provided in Supporting Information. Williamson ether synthesis was performed for alkylation reaction to obtain 1,2-bis(octyloxy)benzene (**2**); a mild base potassium carbonate was used to deprotonate the alkoxy group. Then, 1-bromooctane was slowly added to the reaction medium to give compound **2**. Starting from compound **2**, fuming nitric acid addition was performed to obtain 1,2-dinitro-4,5-bis(octyloxy)benzene (**3**), a ring closure reaction was performed using compound **3**, sodium azide, and triphenylphosphine to obtain benzo[*c*] [1,2,5]oxadiazole main core, compound 5,6-bis(octyloxy)benzo[*c*] [1,2,5]oxadiazole (**4**) successfully. The bromination method with molecular bromine was used to synthesize compound 4,7-dibromo-5,6-bis(octyloxy)benzo[*c*] [1,2,5] oxadiazole (**5**). To obtain 5,6-bis(octyloxy)-4,7-di(thiophen-2-yl)benzo [*c*] [1,2,5]oxadiazole (**8**), Stille coupling of tributyl(thiophen-2-yl) stannane (**7**) and compound **5** was used. After the bromination of compound **8** by N-bromosuccinimide, the target monomer **M1** was successfully synthesized. The synthetic pathway of **M2** consists of the same reactions in a different order. Alkylation was performed at the fourth step instead of the first step to avoid side substitution reactions during the ring-closure reaction since the alkyl group contains the primary halogen group [34–37]. Monomers **M1** and **M2**, were then polymerized with 2,5-bis(trimethylstannyl)thiophene by Stille coupling to obtain **POxT** (Mn = 10 kDa, PDI = 1.40) and **POxT-Br** [38] (Mn = 10 kDa, PDI = 1.70). Finally, post-polymerization of **POxT-Br** with thioacetic acid was performed, and **POxT-SH** was obtained [39] (Mn = 9 kDa, PDI = 1.56) (Scheme 1). The structures of the compounds and monomers were determined by NMR spectroscopy. Additionally, high-resolution mass spectrometry (HRMS) supported the structural analysis of novel compounds. Finally, the structures of polymers were determined by both IR and NMR spectroscopy. Solubility of all polymers in common organic solvents such as chloroform, tetrahydrofuran, and chlorobenzene are excellent.

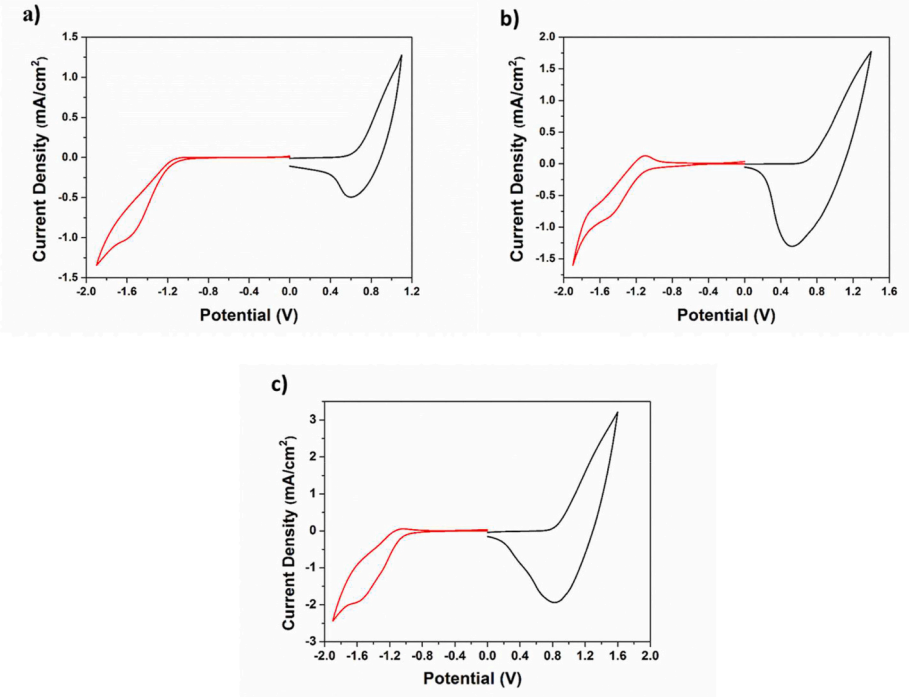

Fig. 1. Cyclic voltammograms of a) **POxT**, b) **POxT-Br** and c) **POxT-SH**.

Synthesis of POxT; In a 25 mL schlenk tube 0.170 g **M1** (243 μmol), 0.100 g **D1** (243 μmol) and 6.0 mg tri(*o*-tolyl)phosphine ($(CH_3C_6H_4)_3P$) (19 μmol) were added. Schlenk tube was vacuumed for 30 min. And then inert gas (N_2) was allowed to pass through the schlenk tube to remove possible oxygen and humidity residues. This process was repeated 3 times. 8 mL of dry toluene ($C_6H_5CH_3$) was added under an N_2 atmosphere, and the temperature was set to 60 °C. The mixture was degassed for 1 h. Then 5.0 mg tris(dibenzylideneacetone)dipalladium(0) ($Pd_2(dba)_3$) (5 μmol) were added to reaction mixture and temperature was raised to 110 °C. The reaction was monitored with TLC control. After 3 h, the reaction mixture was poured into the cold MeOH, and the crude polymer was precipitated. Then, 100 mg of palladium scavenger (3-(Diethylenetriamino)propyl-functionalized silica gel) was added and stirred for 1 h. The crude polymer was then filtrated and collected. The crude polymer was washed with Soxhlet apparatus with an order of methanol, acetone, hexane, and chloroform solvents. Chloroform fragment was collected. Chloroform was evaporated under reduced pressure, and **POxT** was collected (117 mg, 80% yield). ($CHCl_3$ fraction 77 mg, C_6H_5Cl fraction 40 mg) ^{1}H NMR (400 MHz, $CDCl_3$, δ: ppm) 8.40-8.00 (aromatic region), 4.30-3.90 (O–CH_2), 2.10-0.85 (alkyl region). GPC Result of $CHCl_3$ fraction: Mn = 10 kDa, Mw = 14 kDa PDI = 1.40

Synthesis of POxT-Br; In a 25 mL schlenk tube 0.220 g **M2** (257 μmol), 0.106 g **D1** (257 μmol) and 7.0 mg tri(*o*-tolyl)phosphine ($(CH_3C_6H_4)_3P$) (21 μmol) were added. The schlenk tube was vacuumed for 30 min, and then inert gas (N_2) was allowed to pass through the schlenk tube to remove possible oxygen and humidity residues. This process was repeated three times. 8 mL of dry toluene ($C_6H_5CH_3$) were added under an N_2 atmosphere, and the temperature was set to 60 °C. The mixture was degassed for 1 h. Then 5.0 mg tris(dibenzylideneacetone)dipalladium(0) ($Pd_2(dba)_3$) (5 μmol) were added to the reaction mixture and temperature raised to 110 °C. The reaction was terminated after 3 h with TLC control. The reaction mixture was poured into the cold MeOH, and the crude polymer was precipitated. Then, 100 mg of palladium scavenger (3-(Diethylenetriamino)propyl-functionalized silica gel) was added and stirred for 1 h. The crude polymer was then filtrated and collected. The crude polymer was washed with Soxhlet apparatus with an order of methanol, acetone, hexane, chloroform, and chlorobenzene solvents. Chloroform and chlorobenzene fragments were collected. Chloroform and chlorobenzene were evaporated under reduced pressure, and **POxT-Br** was collected (110 mg, 53% yield). ($CHCl_3$ fraction 100 mg, C_6H_5Cl fraction 10 mg) ^{1}H NMR (400 MHz, $CDCl_3$, δ: ppm) 8.40-8.00 (aromatic region), 4.25-4.00 (O–CH_2), 3.50-3.35 (CH_2–Br), 2.10-1.20 (alkyl region). GPC Result of $CHCl_3$ fraction: Mn = 10 kDa, Mw = 17 kDa PDI = 1.70

Synthesis of POxT-SH; In a 100 mL schlenk tube 28.0 mg **POxT-Br**, and 22.0 mg potassium carbonate (K_2CO_3) (76 μmol) were added. The schlenk tube was vacuumed for 30 min, and then inert gas (N_2) was allowed to pass through the schlenk tube to remove possible oxygen and humidity residues. 15 mL of dry tetrahydrofuran (THF) were added under N_2 atmosphere, and the mixture was stirred for 30 min. Then 6.0 mg thioacetic acid (153 μmol) was added to the reaction mixture, and the temperature was raised to 50 °C. The mixture was stirred for 15 h. After that, 15 ml of methanol was added to the reaction mixture, and the mixture was stirred for another 30 min at 50 °C. The reaction was terminated with the addition of 3 drops of 1 M HCl. Solvents were evaporated under reduced pressure, and remaining solids were re-dissolved with $CHCl_3$, and extraction was performed with $CHCl_3$ and brine. The organic phase was collected and dried over $MgSO_4$. The crude polymer was washed with Soxhlet apparatus with an order of methanol, acetone, hexane, and chloroform solvents. Chloroform fragment was collected. Chloroform was evaporated under reduced pressure, and **POxT-SH** was collected (22 mg, 88% yield). Residual bromine was observed on the thiol modified bromine according to ^{1}H NMR spectroscopy. ^{1}H NMR (400 MHz, $CDCl_3$, δ: ppm) 8.50-8.05 (aromatic region), 4.25-4.00 (O–CH_2), 3.50-3.35 (CH_2–Br), 2.40-2.20 (CH_2-SH),2.10-1.20 (alkyl region). GPC Result of $CHCl_3$ fraction: Mn = 9 kDa, Mw = 14 kDa PDI = 1.56

2.2. Optical and electrochemical characterizations

In order to investigate the electrochemical properties of polymers cyclic voltammetry studies were performed. As it is depicted in Fig. 1, which represents the cyclic voltammograms of **POxT**, **POxT-Br**, and **POxT-SH** recorded at a scan rate of 100 mV/s, all polymers feature

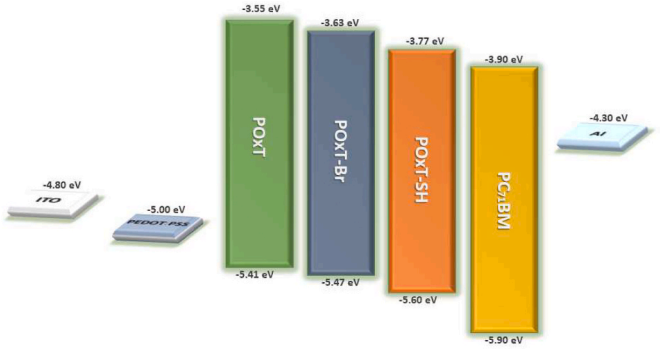

Fig. 2. Energy level diagram of OSCs based on **POxT**, **POxT-Br**, and **POxT-SH**.

ambipolar character. Highest occupied molecular orbital (HOMO) and lowest unoccupied molecular orbital (LUMO) energy levels were calculated using Equations (1) and 2).

$$\mathrm{HOMO} = -(4.75 + \mathrm{E}^{\mathrm{ox}}{}_{\mathrm{onset}}) \quad \text{Eq. (1)}$$

$$\mathrm{LUMO} = -(4.75 + \mathrm{E}^{\mathrm{red}}{}_{\mathrm{onset}}) \quad \text{Eq. (2)}$$

Electronic bandgap (E_g^{el}) equals to the energy gap between the HOMO and LUMO, which were calculated as to be 1.86, 1.84, and 1.83 eV for **POxT, POxT-Br**, and **POxT-SH**, respectively. The results exhibit that Br and SH modifications on side chain do not alter the electrochemical properties significantly, where such characteristic of conjugated polymers was also reported for the similar modifications of EDOT in literature [40,41].

The energy level diagram illustrated in Fig. 2 proves that the corresponding organic solar cells possess suitable HOMO and LUMO offsets to drive the charge transfer between the polymer and $PC_{71}BM$ molecules.

UV–Vis absorption spectra of the polymers are illustrated in Fig. 3. Red shifted absorption was observed in thin film spectra of all polymers compared to solution absorptions due to aggregation of polymers in thin film form. The maximum absorption wavelengths (λ_{max}) values corresponding to π-π* transitions of **POxT, POxT-Br,** and **POxT-SH** were determined as 650 nm, 605 nm, and 610 nm, respectively. Optical band gap (E_g^{op}) values of polymers were calculated using the onset λ_{max}^{onset} values of π-π* transitions and Equation (3), which were determined as 1.68, 1.71 and 1.71 eV for **POxT, POxT-Br** and **POxT-SH**, respectively. The optical data of the polymers are tabulated in Table 1 in comparison with each other. The results demonstrate that electronic band gap values surpass optical band gap values for each polymer, due to the interfacial barrier for charge injection and free-charge formation [42].

$$E_g^{op} = hc/\lambda_{max}^{onset} \quad \text{Eq. (3)}$$

2.3. Nanoparticle synthesis method

Gold nanoparticles (Au NPs) were synthesized by pulsed laser ablation in the liquid method [43,44]. Au-NPs were produced by a nanosecond pulsed Nd:YLF laser (Empower Q-Switched Laser, Spectra Physics) that operates at 527 nm wavelength, 100 ns pulse duration and 1 kHz repetition rate. The target and cuvette were cleaned with distilled water in an ultrasonic bath for 3 min before the synthesis. The bulk gold target was immersed into pure 10 mL methanol and placed at the bottom of a quartz cuvette. The laser was focused with a plano-convex lens with 50 mm focal length. The laser was operated at 16 W power corresponding to 16 mJ pulse energy, and the ablation time was 5 min. To

Table 1
Summary of electrochemical and optical studies of polymers.

	HOMO (eV)	LUMO (eV)	E_g^{el} (eV)	λ_{max} (nm)	λ_{max}^{onset}(nm)	E_g^{op} (eV)
POxT	−5.41	−3.55	1.86	650	740	1.68
POxT-Br	−5.47	−3.63	1.84	605	725	1.71
POxT-SH	−5.60	−3.77	1.83	610	725	1.71

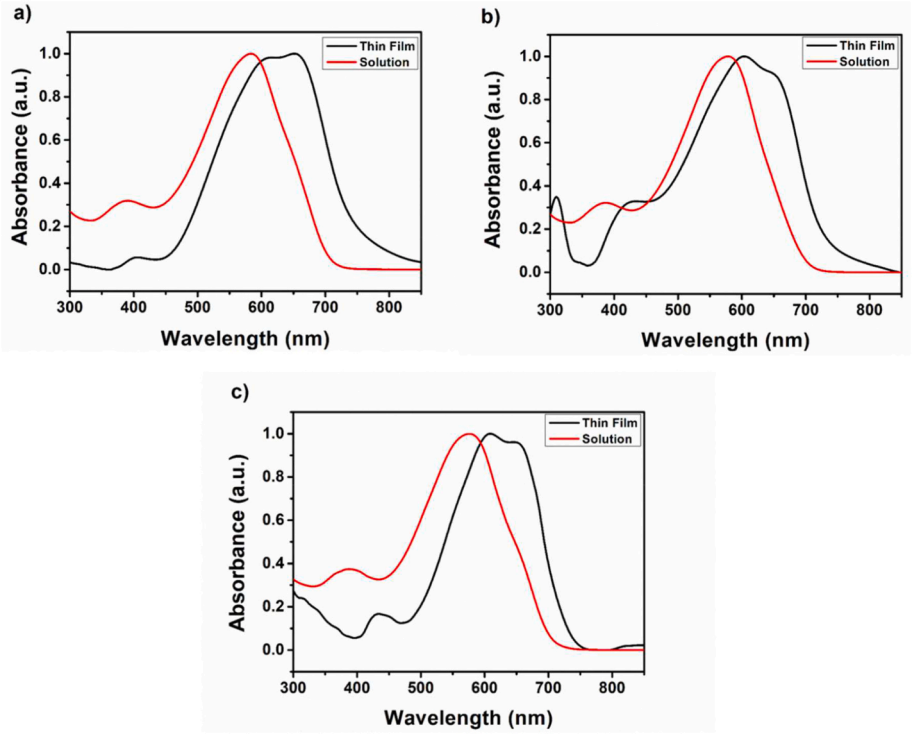

Fig. 3. Normalized UV–Vis absorption spectra of a) **POxT**, b) **POxT-Br** and c) **POxT-SH**.

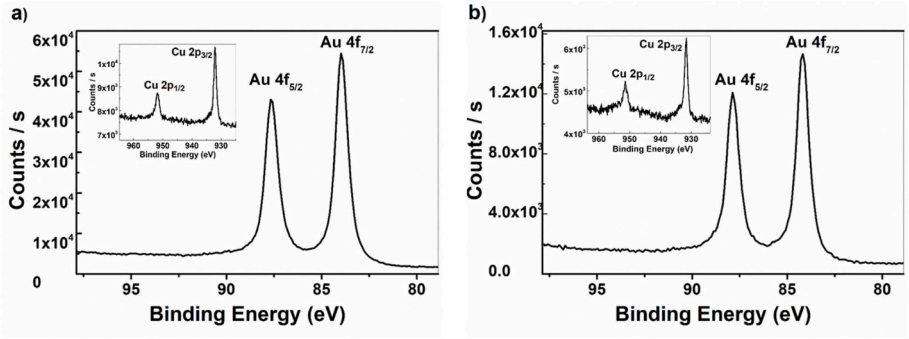

Fig. 4. XPS spectra of (a) the target sample and (b) the nanocolloidal.

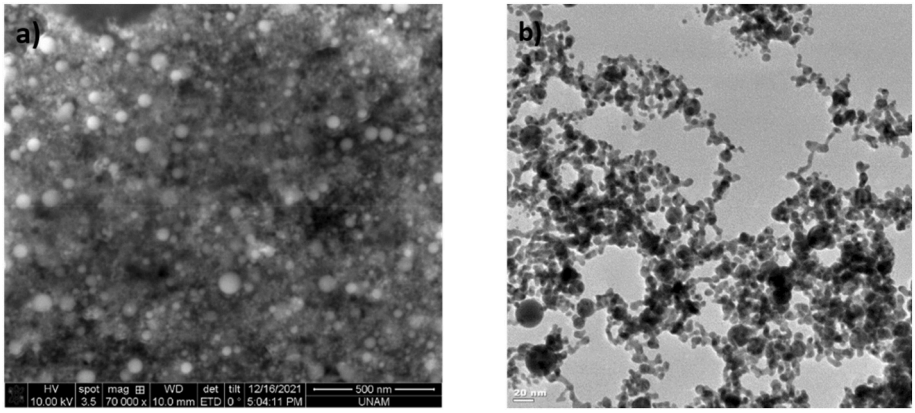

Fig. 5. a) SEM and b) TEM images of nanocolloidal solution generated by laser ablation.

increase the absorption of incident light through the nanocomposite of the solar cell, we increased the nano-colloidal concentration per unit volume. The resulting colloid had around 0.512 mg/mL concentration and had dark purple color. The aggregation in the synthesized colloid was observed due to very high concentration and thus, these nano-colloidal solutions were used immediately in solar cell fabrication.

2.4. Characterization of gold nanoparticles

The characterization of the elemental composition of the synthesized nanoparticles and the used sample was performed via X-ray photoelectron spectroscopy (XPS). The measurements were carried out by using the monochromatic instrument K-Alpha (Thermo Scientific) which operates at 12 kV and 2.5 mA. The sample was prepared by dripping the colloid onto a Si substrate. The formation of nanoparticles and their morphology were confirmed by scanning electron microscope (SEM, Quanta 200 FEG, FEI Instruments) imaging. The imaging process was also repeated using a high-resolution transmission electron microscope (HR-TEM) with an operating voltage of 300 kV by using the FEI-Tecnai G2 F30 TEM instrument. The samples were prepared by drop-casting the solutions onto carbon-coated TEM grids. To verify the surface plasmon absorption properties of the nanocolloidal, an absorption analysis was carried out using UV–Vis–NIR Spectrophotometer (Varian, Cary 5000 UV–Vis–NIR Spectrophotometer), at a wavelength range of 400–800 nm.

The composition of the target sample was determined by XPS analysis. The results of the XPS analysis are illustrated in Fig. 4a. The sample has Au $4f_{7/2}$ peak at 84.15 eV and Au $4f_{5/2}$ peak at 87.65 eV [45]. For the copper side, the sample presents the peaks at 932.2 eV and 951.9 eV for Cu $2p_{3/2}$ and Cu $2p_{1/2}$, respectively. These results show that Au and Cu are in their metallic forms and there is no bonding or alloy formation. From the integrated areas, it is determined that the sample consists of

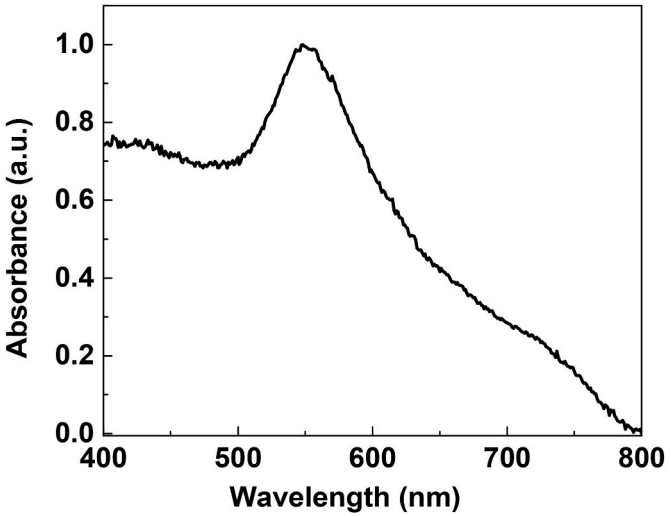

Fig. 6. UV–Vis absorbance graph of Au NPs.

90% of gold and 10% of copper, respectively. The sample is determined to be gold-rich sample with copper addition. The XPS spectra of the synthesized nanoparticles were also recorded (see Fig. 4b), showing the peaks of Au $4f_{7/2}$ and Au $4f_{5/2}$ at 84.35 eV and 87.85 eV, respectively. In addition, the nano-colloidal synthesized by laser ablation also features Cu $2p_{3/2}$ and $2p_{1/2}$ peaks at 931.5 eV and 951.2 eV, respectively. The integrated areas of gold and copper scan data show that the composition of the nano-colloidal is at the same level as the target sample.

Fig. 5a presents the SEM image of nanoparticles generated by laser ablation of the gold-rich target in methanol, which reveals the spherical

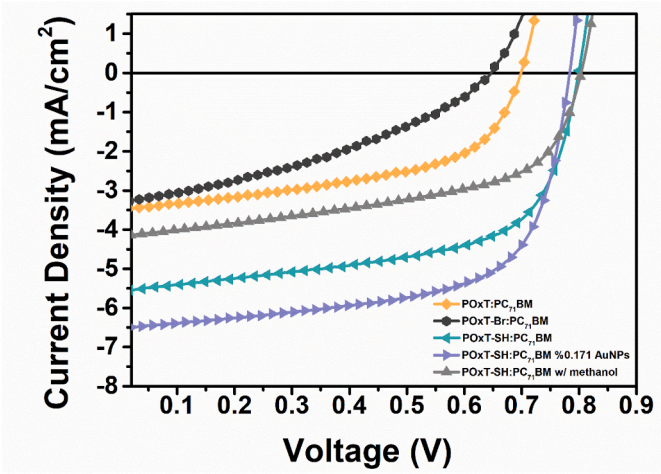

Fig. 7. The J-V curves of the OSCs based on **POxT**, **POxT-Br**, **POxT-SH** with and without Au NPs.

Table 2
Summary of photovoltaic parameters.

	V_{OC} (V)	J_{SC} (mA/cm^2)	FF (%)	PCE (%)
POxT: $PC_{71}BM$	0.70	3.49	52.8	1.29
POxT-Br: $PC_{71}BM$	0.65	3.30	36.5	0.78
POxT-SH: $PC_{71}BM$	0.80	5.57	60.9	2.71
POxT-SH: $PC_{71}BM$, %0.085 AuNPs	0.78	6.42	55.0	2.76
POxT-SH: $PC_{71}BM$, %0.171 AuNPs by mass	0.78	6.52	64.5	3.29
POxT-SH: $PC_{71}BM$, %0.513 AuNPs	0.80	4.04	51.0	1.65
POxT-SH: $PC_{71}BM$, methanol	0.80	4.17	54.3	1.82

shape of nanoparticles with sub 50 nm of diameter. TEM image (see Fig. 5b) of the nanoparticles also confirms the spherical shape of nanoparticles synthesized by laser ablation in the liquid process as expected. The Au NPs are below 50 nm in size, but most of those nanoparticles are smaller than the region of 10 nm. Some aggregation can be observed, but this is due to the high concentration of nanoparticles in the colloid and the absence of chemical stabilizers. As a result of the high laser fluence used during synthesis, a broad size range occurs.

Fig. 6 illustrates the absorption properties of nanoparticles in the visible region, where the surface plasmon absorption (SPA) peak is located at 548 nm. As there is no additional SPA peak around 600 nm, which is specific to copper nanoparticles [46], the corresponding colloidal solution can be considered as Au NP solution. Hence, the SPA peak indicates that these nanoparticles can be used to amplify the photocurrent production of organic solar cells upon incorporation (see Fig. 7).

2.5. Photovoltaic characterizations

Organic solar cells were fabricated using conventional device architecture of ITO/PEDOT:PSS/active layer/LiF/Al. The active layer contains a polymeric p-type donor material and a fullerene-based n-type acceptor material ($PC_{71}BM$). In this study, gold nanoparticles were embedded in the active layer to achieve surface plasmonic absorption for higher photocurrent production without increasing the active layer thickness. Morphological and photovoltaic characterizations were performed through the fabrication of devices by processing active layer solutions with and without gold nanoparticle incorporation. Solvent, blend concentration, donor:acceptor ratio, and active layer thickness optimizations were performed for **POxT**, **POxT-Br**, and **POxT-SH** based organic solar cells. Optimized device performance was obtained using a donor:acceptor weight ratio of 1:2 and spin coating the mixture at a total concentration of 15 mg/mL. Polymer **POxT** based OSCs displayed a PCE of 1.29% with a V_{OC} of 0.70 V, J_{SC} of 3.49 mA/cm^2 and a FF of 52.8% (Fig. 7). For the brominated polymer **POxT-Br** based OSCs, PCE value decreased to 0.78% through a significant decrease in FF values. Large bromine disrupts the chain packing of the polymer which will be detailed in morphology studies. In addition to this, it is known that bromine end groups create hole traps in the polymer thus leading to a loss in performance of OSCs [47]. Highlighted outcomes of the photovoltaic characterizations are tabulated in Table 2.

As Table 2 represents, thiol modification of **POxT** enhanced the power conversion efficiency through a rise in both fill factor and short-circuit current density values. Although, the bromine is not completely substituted by the sulfhydryl group, **POxT-SH** has showed superior photovoltaic performance when compared **POxT** and **POxT-Br** due to formation of well-defined active layer morphology with aligned polymer domains. For organic photovoltaic applications, the effect of thiol groups on the overall performance of BHJ-OSC devices remains unrevealed. Complete substitution of bromine into thiol groups can boost the photovoltaic performance since it eliminates the risk of creation of hole traps and morphological distortions that may cause from large bromine atom. Regarding photovoltaic performance, the superiority of thiol-functionalized polymers is related to the strong covalent interaction with the metal contact upon utilization as the interfacial layer. Such interaction facilitates low contact resistance and strong interfacial adhesion that could assist the charge extraction at the metal electrode, and the improved device stability in various atmospheres and temperatures. Although this is an advantage specific to inverted device architecture, it could also drive the formation of well-defined active layer morphology with aligned polymer domains [48–50]. For organic photovoltaic applications, the effect of thiol groups on the overall performance of BHJ-OSC devices remains unrevealed. In this manner, this study reports a new molecular design approach to present the amplified PCE values upon thiol modification on the polymer pendant group.

This work also proposes another novel approach, the use of ligand stabilizer-free Au NPs inside the active layer, which is to tackle the diminished charge diffusion and extraction caused by the trap-forming ligand incorporation. However, such application would drive the aggregation of the NPs which impedes the homogeneous distribution and formation of non-ideal active layer morphology [51,52]. Aggregation of metal NPs in active layer leads to formation of recombination centers and high leakage current. Kymakis reported the incorporation of tetraoctylammonium bromide coated Au NPs in active layer and confirmed that incorporation of coated Au NPs to the active layer results in attenuated photovoltaic parameters due to NP assisted recombination in spite of the enhanced light absorption [53].

Decreasing the distance between the NP and polymer in the active layer is a proposed way to impede NP assisted recombination [53]. In this regard, the thiol-incorporated molecular design of **POxT-SH** is expected to stabilize and homogeneously align the Au NPs upon the covalent interaction in between. Hence, the goal is to enhance the light-harvesting upon Au NP incorporation with an optimum active layer morphology.

Gold nanoparticles were embedded in active layers composed of **POxT-SH**:$PC_{71}BM$ with different weight ratios. The extent of Au NP incorporation was also optimized in terms of the photovoltaic performance of **POxT-SH.** Upon optimization of the Au NP concentration, incorporation of 0.171% by mass was determined to exhibit the highest photovoltaic performance for **POxT-SH**-based organic solar cells, with J_{SC}, V_{OC}, FF and PCE values of 6.52 mA/cm^2, 0.78 V, 64.5% and 3.29%, respectively. J_{SC} and FF improvements are leading factors for the device performance enhancement for **POxT-SH** and Au NP incorporated OSCs. It is concluded that the inclusion of Au NPs enhances the charge carrier generation and transport via the plasmonic effect and morphology improvement.

When the Au NP concentration was increased to 0.513% by mass, PCE value was lowered from 3.29% to 1.65% due to generation of hot

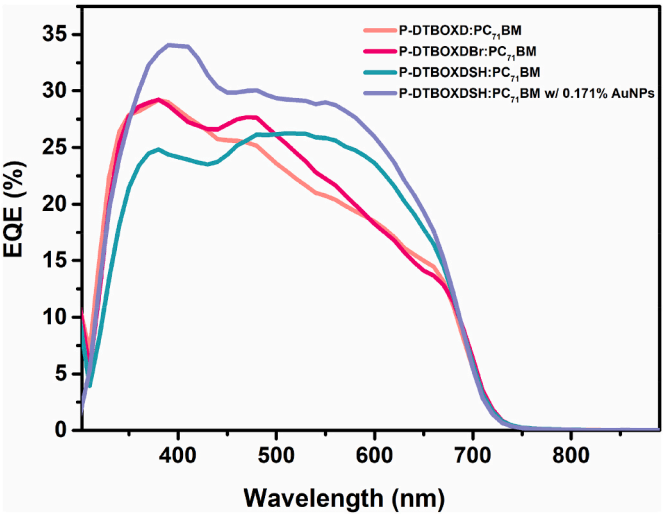

Fig. 8. The EQE curves of the champion solar cells based on **POxT**, **POxT-Br**, **POxT-SH** with and without Au NPs.

spots leading to disturbed exciton and plasmon interaction. In addition to electrical effects, excessive Au NP addition significantly lowers the FF values, which is a consequence of disturbed morphology [54].

Solvent selection is critical since solvents used in dissolution of polymer fullerene blends do not disperse Au nanoparticles. In this study, Au nanoparticles were dispersed in methanol. Methanol is commonly used as a surface treatment agent to improve the efficiencies of organic solar cells [55,56]. To understand the individual contribution of Au NPs dissolved in methanol to enhance the photovoltaic performance of the polymer, pure methanol treatment was also performed for **POxT-SH** based organic solar cells. The results clearly display that pure methanol treatment significantly lowers the PCE values, in contrast with the results achieved for Au NP incorporation. Hence, the enhanced photovoltaic performance of **POxT-SH** could be directly attributed to the Au NP addition and the polymer-NP interactions.

In the light of photovoltaic studies, thiol functionalization augmented the efficiency from 1.29% to 2.71%. Au NP inclusion to the active layer boosted the efficiency further to 3.29%.

To verify the J_{SC} values determined via photovoltaic studies, external quantum efficiency (EQE) characterizations of the fabricated solar cells were carried out, where EQE is a measure of electrons produced per incident photon interacting with the solar cell. Fig. 8 clearly displays the increase in photocurrent production through thiol modification and Au NP incorporation.

2.6. Morphological studies

Morphological and topographical analyses were performed using transmission electron microscopy (TEM) and atomic force microscopy (AFM). Fig. 9a illustrates the TEM view of **POxT** based active layer, possessing large area acceptor-rich domains with no bicontinuity. Fig. 9b exhibits brominated polymer **POxT-Br**:$PC_{71}BM$ blend morphology featuring no phase separation with the insignificant donor: acceptor domains, which may lead to inefficient charge transfer and

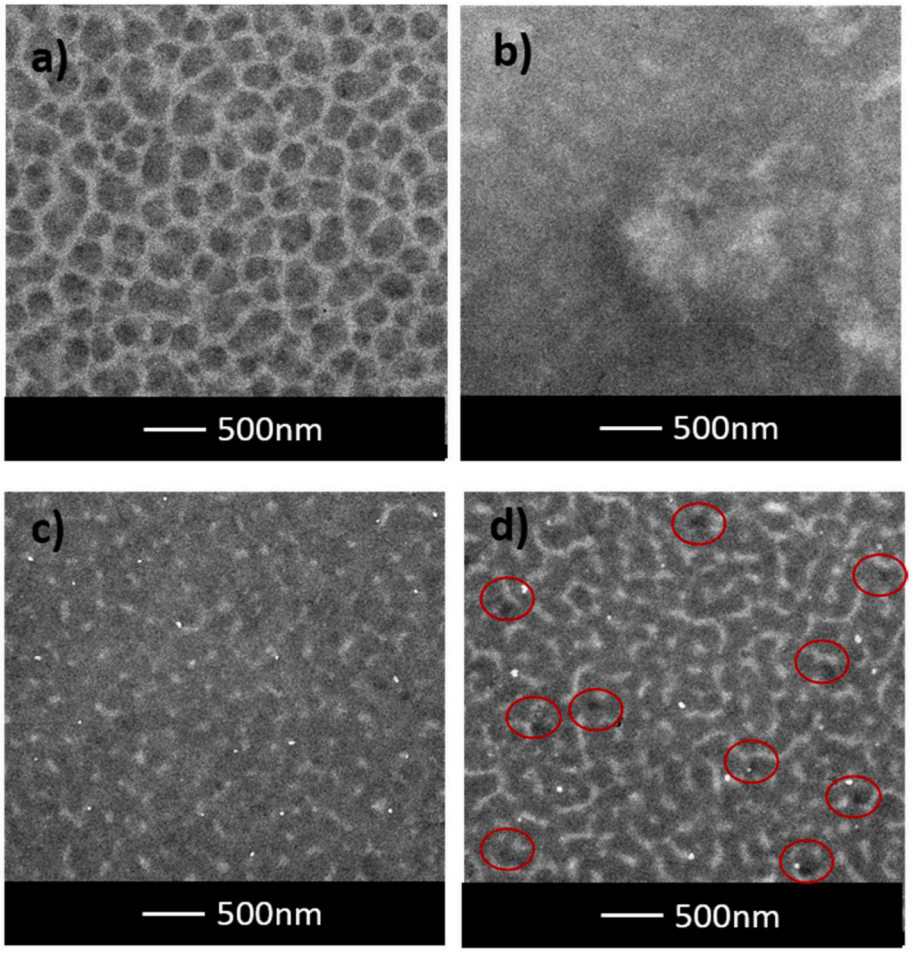

Fig. 9. TEM images of a) POxT: $PC_{71}BM$, b) POxT-Br: $PC_{71}BM$, c) POxT-SH: $PC_{71}BM$ and d) POxT-SH: $PC_{71}BM$ and 0.171% AuNPs by mass films.

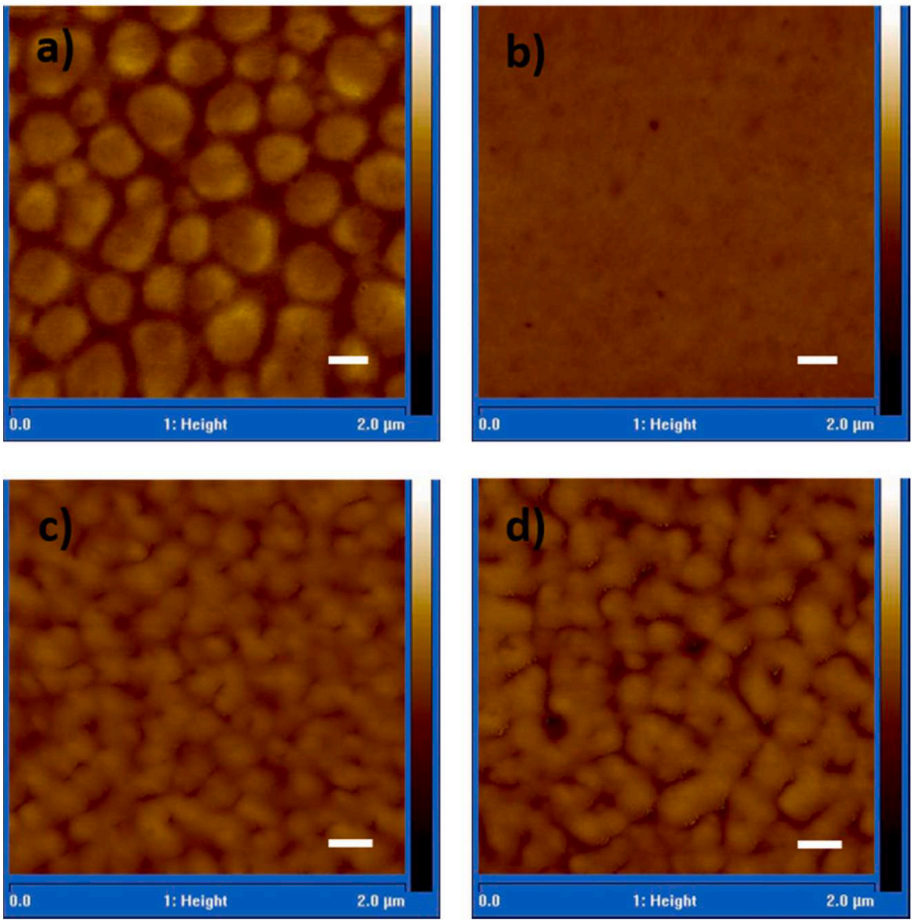

Fig. 10. AFM images of a) P-DTBOXD: $PC_{71}BM$, b) POxT-Br: $PC_{71}BM$, c) POxT-SH: $PC_{71}BM$ ve d) POxT-SH: $PC_{71}BM$ and 0.171% AuNPs by mass films (Scale bar is 200 nm).

extraction. Large bromine disrupts the active layer morphology thus leading to lower photovoltaic performance [47].

Fig. 9c stands for the TEM image of **POXT-SH**:$PC_{71}BM$-based film, in which the formation of bicontinuious donor and acceptor domains and narrower polymer fibrils easing the exciton diffusion to the donor acceptor interface are observed. Well-defined percolation pathways which is absent for **POxT** comprising film, are being established. The superiority of **POxT-SH**:$PC_{71}BM$-based solar cells in terms of performance could be correlated with the enhanced charge extraction efficiency with the improved active layer morphology.

The morphology of 0.171% Au NP by mass incorporated **POxT-SH**: $PC_{71}BM$ blend-based active layer is illustrated in Fig. 9d, and the Au NP clusters distributed are circled in red. Fig. 9d presents the formation of wider polymer domains upon 0.171% Au NP by mass incorporation, where the bicontinuity is improved significantly. As mentioned previously, such modification in the film morphology yields higher efficiency of charge extraction, with enhanced PCE values. The corresponding image also exhibits the polymer-gold interactions, where the Au NPs are distributed near the polymer domains. Therefore, this could lead to the uniform alignment of the polymer domains, which could also be linked to polymers percolating effectively. Consequently, morphological aspects co-elevate the PCE values with the increased light-harvesting properties due to plasmonic effect of Au NPs.

The surface roughness values were determined as 2.10 nm, 1.54 nm, 0.57 nm and 2.94 nm for **POxT**: $PC_{71}BM$, **POxT-Br**: $PC_{71}BM$, **POXT-SH**: $PC_{71}BM$ and Au NP incorporated **POXT-SH**: $PC_{71}BM$, respectively, via AFM analysis. The corresponding AFM images are illustrated in Fig. 10a, b, c, and d. Higher roughness results in increased surface area of the active layer, where higher number of photons are absorbed. In addition, the absorption efficiency is improved through decreased internal resistance and enhanced light trapping [57]. As a result, a higher roughness value of Au NP incorporated **POxT-SH**: $PC_{71}BM$ films contribute to the superior J_{SC} value of the corresponding value.

3. Conclusion

In this study, benzoxadiazole bearing conjugated polymer and its brominated and thiol modified derivatives were successfully synthesized. The electrochemical and optical characterizations of the polymers were performed followed by their comparative photovoltaic and morphological studies. Polymers exhibited no significant difference in terms of their optoelectronic properties, as bromine and thiol groups do not contribute to the backbone conjugation. To utilize the covalent interaction between gold and thiol groups and surface plasmonic absorption of metal nanoparticles, gold nanoparticle incorporation to the active layer to achieve augmented power conversion efficiency values were performed. To this goal, gold nanoparticles were synthesized via the laser ablation method in methanol without any ligand stabilization, which was added to the active layer solutions at different concentrations. In addition to the novelty of the use of ligand-free gold nanoparticles in the active layer, this work also emphasizes the positive impact on the photovoltaic performance of the thiol modification for the first time, increasing the PCE from 1.29% to 2.71%, compared to non-modified **POxT**, through a rise in J_{SC} and V_{OC} values, which could be correlated with the formation of interpenetrated bicontinuous active layer morphology upon the use of thiol modified **POxT-SH** in the donor-

acceptor blend. Further improvement of the photovoltaic performance was achieved via gold nanoparticle incorporation at an optimum concentration of 0.171% by mass in **POxT-SH**-based active layer, assisting the formation of well-established percolation pathways and the solar cells achieving a J_{SC} of 6.52 mA/cm^2 and PCE to 3.29%. Hence, we conclude that the interaction between thiol groups and gold nanoparticles imparts strong light harvesting capabilities in the blend yielding enhanced photocurrent production, proven by the 21.4% increase in the PCE compared to the pristine donor-acceptor blend of the same polymer.

Associated content

General measurement and characterization; synthesis of molecules, monomers, and polymers; fabrication of BHJ devices; ^{1}H and ^{13}C NMR spectra of molecules and monomers; HRMS spectra of novel molecules; ^{1}H NMR and IR spectra of polymers.

Author contributions

O.K. designed the experiments, synthesized the molecules, polymers and characterized them. E.A. and M.C.E. performed measurements and characterizations of solar devices. D.C. performed electronic and photovoltaic measurements and characterizations. S.G. assisted to molecule synthesis. U.T. synthesized gold nano-particles and characterized them. S.C.C. conceptualized the study and designed the experiments. G.H.O. revised the manuscript. B.O. supervised gold-nanoparticle synthesis and A.C. supervised the whole research work. The manuscript was written through contributions of all authors. All authors have given approval to the final version of the manuscript.

Declaration of competing interest

The authors declare that they have no known competing financial interests or personal relationships that could have appeared to influence the work reported in this paper.

Data availability

Data will be made available on request.

Acknowledgment

We are thankful for financial support from the Scientific and Technological Research Council of Türkiye (TUBITAK) with project number 118Z738.

Appendix A. Supplementary data

Supplementary data to this article can be found online at https://doi.org/10.1016/j.dyepig.2022.110818.

References

[1] Simon JJ, Escoubas L, Monestier F, Torchio P, Flory F. Optical properties engineering for organic solar cells. Int J Mater Prod Technol 2009;34:469–87. https://doi.org/10.1504/IJMPT.2009.025001.
[2] Sun C, Xia R, Shi H, Yao H, Liu X, Hou J, et al. Heat-insulating multifunctional semitransparent polymer solar cells. Joule 2018;2:1816–26. https://doi.org/10.1016/j.joule.2018.06.006.
[3] Yue W, Huang X, Yuan J, Ma W, Krebs FC, Yu D. A novel benzodipyrrolidone-based low band gap polymer for organic solar cells. J Mater Chem 2013;1:10116–9. https://doi.org/10.1039/c3ta12701j.
[4] Li G, Zhu R, Yang Y. Polymer solar cells. Nat Photonics 2012;6:153–61. https://doi.org/10.1038/nphoton.2012.11.
[5] Blom PWM, Mihailetchi VD, Koster LJA, Markov DE. Device physics of polymer: Fullerene bulk heterojunction solar cells. Adv Mater 2007;19:1551–66. https://doi.org/10.1002/adma.200601093.
[6] Jean R. Molecular bulk heterojunctions: an emerging approach to organic solar cells. Acc Chem Res 2009;42:1719–30. https://doi.org/10.1021/ar900041b.
[7] Wang DH, Park KH, Seo JH, Seifter J, Jeon JH, Kim JK, et al. Enhanced power conversion efficiency in PCDTBT/PC 70 BM bulk heterojunction photovoltaic devices with embedded silver nanoparticle clusters. Adv Energy Mater 2011;1:766–70. https://doi.org/10.1002/aenm.201100347.
[8] Park SH, Roy A, Beaupré S, Cho S, Coates N, Moon JS, et al. Bulk heterojunction solar cells with internal quantum efficiency approaching 100%. Nat Photonics 2009;3:297–303. https://doi.org/10.1038/nphoton.2009.69.
[9] Wang DH, Park KH, Seo JH, Seifter J, Jeon JH, Kim JK, et al. Enhanced power conversion effi ciency in PCDTBT/PC 70 BM bulk heterojunction photovoltaic devices with embedded silver nanoparticle clusters. 766–70, https://doi.org/10.1002/aenm.201100347; 2011.
[10] Kang MG, Xu T, Park HJ, Luo X, Guo LJ. Efficiency enhancement of organic solar cells using transparent plasmonic Ag nanowire electrodes. Adv Mater 2010;22:4378–83. https://doi.org/10.1002/adma.201001395.
[11] Lindquist NC, Luhman WA, Oh SH, Holmes RJ. Plasmonic nanocavity arrays for enhanced efficiency in organic photovoltaic cells. Appl Phys Lett 2008;93:67–70. https://doi.org/10.1063/1.2988287.
[12] Gao H, Meng J, Sun J, Deng J. Enhanced performance of polymer solar cells based on P3HT:PCBM via incorporating Au nanoparticles prepared by the micellar method. J Mater Sci Mater Electron 2020;31. https://doi.org/10.1007/s10854-020-03626-x. 10760–7.
[13] Bao ZY, Liu S, Hou Y, Shang A, Yan F, Wu Y, et al. Hollow Au nanorattles for boosting the performance of organic photovoltaics. J Mater Chem 2019;7:26797–803. https://doi.org/10.1039/c9ta07974b.
[14] Shin J, Song M, Hafeez H, Jeusraj PJ, Kim DH, Lee JC, et al. Harvesting near- and far-field plasmonic enhancements from large size gold nanoparticles for improved performance in organic bulk heterojunction solar cells. Org Electron 2019;66:94–101. https://doi.org/10.1016/j.orgel.2018.12.024.
[15] Ali AM, Said DA, Khayyat M, Boustimi M, Seoudi R. Improving the efficiency of the organic solar cell (CuPc/C60) via PEDOT: PSS as a photoconductor layer doped by silver nanoparticles. Results Phys 2020;16:102819. https://doi.org/10.1016/j.rinp.2019.102819.
[16] Said DA, Ali AM, Khayyat MM, Boustimi M, Loulou M, Seoudi R. A study of the influence of plasmonic resonance of gold nanoparticle doped PEDOT: PSS on the performance of organic solar cells based on CuPc/C60. Heliyon 2019;5:e02675. https://doi.org/10.1016/j.heliyon.2019.e02675.
[17] Jheng JY, Sah PT, Chang WC, Chen JH, Chan LH. Decahedral gold nanoparticles for enhancing performance of polymer solar cells. Dyes Pigments 2017;138:83–9. https://doi.org/10.1016/j.dyepig.2016.11.027.
[18] Babaei Z, Rezaei B, Pisheh MK, Afshar-Taromi F. In situ synthesis of gold/silver nanoparticles and polyaniline as buffer layer in polymer solar cells. Mater Chem Phys 2020;248:122879. https://doi.org/10.1016/j.matchemphys.2020.122879.
[19] Sun Y, Ren G, Han S, Zhang X, Liu C, Li Z, et al. Improving light harvesting and charge extraction of polymer solar cells upon buffer layer doping. Sol Energy 2020;202:80–5. https://doi.org/10.1016/j.solener.2020.03.105.
[20] Gao Y, Jin F, Su Z, Zhao H, Luo Y, Chu B, et al. Cooperative plasmon enhanced organic solar cells with thermal coevaporated Au and Ag nanoparticles. Org Electron 2017;48:336–41. https://doi.org/10.1016/j.orgel.2017.06.003.
[21] Yao K, Zhong H, Liu Z, Xiong M, Leng S, Zhang J, et al. Plasmonic metal nanoparticles with core-bishell structure for high-performance organic and perovskite solar cells. ACS Nano 2019;13:5397–409. https://doi.org/10.1021/acsnano.9b00135.
[22] Kaçuş H, Aydoğan Biber M, Metin Sevim M. The power conversion efficiency optimization of the solar cells by doping of (Au:Ag) nanoparticles into P3HT:PCBM active layer prepared with chlorobenzene and chloroform solvents. Mater Res Express 2019;6. https://doi.org/10.1088/2053-1591/ab309a.
[23] Chuang MK, Lin CH, Chen FC. Accumulated plasmonic effects of gold nanoparticle–decorated PEGylated graphene oxides in organic light-emitting diodes. Dyes Pigments 2020;180:108412. https://doi.org/10.1016/j.dyepig.2020.108412.
[24] Du Z, Yu T, He W, Yurtsever A, Izquierdo R, Jafari M, et al. Enhancing efficiency of nonfullerene organic solar cells via using polyelectrolyte-coated plasmonic gold nanorods as rear interfacial modifiers. ACS Appl Mater Interfaces 2022;14:16185–96. https://doi.org/10.1021/acsami.1c25223.
[25] Rezaei B, Afshar-Taromi F, Ahmadi Z, Amiri Rigi S, Yousefi N. Enhancement of power conversion efficiency of bulk heterojunction polymer solar cells using core/shell, Au/graphene plasmonic nanostructure. Mater Chem Phys 2019;228:325–35. https://doi.org/10.1016/j.matchemphys.2019.02.084.
[26] Stratakis E, Kymakis E. Nanoparticle-based plasmonic organic photovoltaic devices. Mater Today 2013;16:133–46. https://doi.org/10.1016/j.mattod.2013.04.006.
[27] Kim K, Carroll DL. Roles of Au and Ag nanoparticles in efficiency enhancement of poly(3-octylthiophene)/C 60 bulk heterojunction photovoltaic devices. Appl Phys Lett 2005;87:1–3. https://doi.org/10.1063/1.2128062.
[28] Häkkinen H. The gold–sulfur interface at the nanoscale. Nat Chem 2012;4. https://doi.org/10.1038/nchem.1352.
[29] Ackerson CJ, Jadzinsky PD, Sexton JZ, Bushnell DA, Kornberg RD. Synthesis and bioconjugation of 2 and 3 nm-diameter gold nanoparticles. Bioconjugate Chem 2010;21:214–8. https://doi.org/10.1021/bc900135d.
[30] Bowman MC, Ballard TE, Ackerson CJ, Feldheim DL, Margolis DM, Melander C. Inhibition of HIV fusion with multivalent gold nanoparticles. J Am Chem Soc 2008;130:6896–7. https://doi.org/10.1021/ja710321g.
[31] Patel PC, Giljohann DA, Daniel WL, Zheng D, Prigodich AE, Mirkin CA. Scavenger receptors mediate cellular uptake of polyvalent oligonucleotide-functionalized

gold nanoparticles. Bioconjugate Chem 2010;21:2250–6. https://doi.org/10.1021/bc1002423.
[32] Verma A, Stellacci F. Effect of surface properties on nanoparticle-cell interactions. Small 2010;6:12–21. https://doi.org/10.1002/smll.200901158.
[33] Demers LM, Ginger DS, Park SJ, Li Z, Chung SW, Mirkin CA. Direct patterning of modified oligonucleotides on metals and insulators by dip-pen nanolithography. 80 Science 2002;296:1836–8. https://doi.org/10.1126/science.1071480.
[34] Shopsowitz K, Lelj F, MacLachlan MJ. Regioselectivity in the nitration of dialkoxybenzenes. J Org Chem 2011;76:1285–94. https://doi.org/10.1021/jo102113t.
[35] Bouffard J, Swager TM. Fluorescent conjugated polymers that incorporate substituted 2,1,3-benzooxadiazole and 2,1,3-benzothiadiazole units. Macromolecules 2008;41:5559–62. https://doi.org/10.1021/ma8010679.
[36] Prima DO, Makarov AG, Bagryanskaya IY, Kolesnikov AE, Zargarova LV, Baev DS, et al. Fluorine-Containing n-6 and angular and linear n-6-n' (n, n' = 5, 6, 7) diaza-heterocyclic scaffolds assembled on benzene core in unified way. ChemistrySelect 2019;4:2383–6. https://doi.org/10.1002/slct.201803970.
[37] Goker S, Hizalan G, Kutkan S, Arslan Udum Y, Cirpan A, Toppare L. Incorporation of different conjugated linkers into low band gap polymers based on 5,6-Bis (octyloxy)-2,1,3 benzooxadiazole for tuning optoelectronic properties. J Polym Sci Part A Polym Chem 2016;54:2459–67. https://doi.org/10.1002/pola.28141.
[38] Yuan M, Yang P, Durban MM, Luscombe CK. Low bandgap polymers based on silafluorene containing multifused heptacylic arenes for photovoltaic applications. Macromolecules 2012;45:5934–40. https://doi.org/10.1021/ma300839c.
[39] Han CC, Balakumar R. Mild and efficient methods for the conversion of benzylic bromides to benzylic thiols. Tetrahedron Lett 2006;47:8255–8. https://doi.org/10.1016/j.tetlet.2006.09.093.
[40] Zhang L, Wen Y, Yao Y, Duan X, Xu J, Wang X. Electrosynthesis, characterization, and application of poly(3,4- ethylenedioxythiophene) derivative with a chloromethyl functionality. J Appl Polym Sci 2013;130:2660–70. https://doi.org/10.1002/app.39478.
[41] Balog M, Rayah H, Le Derf F, Sallé M. A versatile building block for EDOT or PEDOT functionalization. New J Chem 2008;32:1183–8. https://doi.org/10.1039/b715568a.
[42] Huo L, Chen HY, Hou J, Chen TL, Yang Y. Low band gap dithieno[3,2-b:2′,3′-d] silole-containing polymers, synthesis, characterization and photovoltaic application. Chem Commun 2009;5570–2. https://doi.org/10.1039/b910443g.
[43] Burzhuev S, Dâna A, Ortaç B. Laser synthesized gold nanoparticles for high sensitive strain gauges. Sensors Actuators, A Phys 2013;203:131–6. https://doi.org/10.1016/j.sna.2013.08.034.
[44] Deniz AE, Vural HA, Ortaç B, Uyar T. Gold nanoparticle/polymer nanofibrous composites by laser ablation and electrospinning. Mater Lett 2011;65:2941–3. https://doi.org/10.1016/j.matlet.2011.06.045.
[45] Arévalo AC, Quintero JH, Rincón SA, Rodriguez J, Ospina R. Gold nanoparticles size distribution by pulsed laser varying the wavelength. J Phys Conf Ser 2019;1418. https://doi.org/10.1088/1742-6596/1418/1/012019.
[46] Liu P, Wang H, Li X, Rui M, Zeng H. Localized surface plasmon resonance of Cu nanoparticles by laser ablation in liquid media. RSC Adv 2015;5:79738–45. https://doi.org/10.1039/c5ra14933a.
[47] Kim Y, Cook S, Kirkpatrick J, Nelson J, Durrant JR, Bradley DDC, et al. Effect of the end group of regioregular poly(3-hexylthiophene) polymers on the performance of polymer/fullerene solar cells. J Phys Chem C 2007;111:8137–41. https://doi.org/10.1021/jp072306z.
[48] Cho JH, Lim JA, Han JT, Jang HW, Lee JL, Cho K. Control of the electrical and adhesion properties of metal/organic interfaces with self-assembled monolayers. Appl Phys Lett 2005;86:1–3. https://doi.org/10.1063/1.1914961.
[49] Yip HL, Hau SK, Baek NS, Jen AKY. Self-assembled monolayer modified ZnO/metal bilayer cathodes for polymer/fullerene bulk-heterojunction solar cells. Appl Phys Lett 2008;92. https://doi.org/10.1063/1.2919524.
[50] Kind H, Bonard JM, Emmenegger C, Nilsson LO, Hernadi K, Maillard-Schaller E, et al. Patterned films of nanotubes using microcontact printing of catalysts. vol. 11, https://doi.org/10.1002/(SICI)1521-4095(199910)11:15<1285::AID-ADMA1285>3.0.CO;2-J; 1999.
[51] Yoon W-J, Jung K-Y, Liu J, Duraisamy T, Revur R, Teixeira FL, et al. Plasmon-enhanced optical absorption and photocurrent in organic bulk heterojunction photovoltaic devices using self-assembled layer of silver nanoparticles. Sol Energy Mater Sol Cells 2010;94:128–32. https://doi.org/10.1016/j.solmat.2009.08.006.
[52] Lee TH, Park SY, Walker B, Ko SJ, Heo J, Woo HY, et al. A universal processing additive for high-performance polymer solar cells. RSC Adv 2017;7:7476–82. https://doi.org/10.1039/c6ra27944a.
[53] Kymakis E, Spyropoulos GD, Fernandes R, Kakavelakis G, Kanaras AG, Stratakis E. Plasmonic bulk heterojunction solar cells: the role of nanoparticle ligand coating. ACS Photonics 2015;2:714–23. https://doi.org/10.1021/acsphotonics.5b00202.
[54] Spyropoulos GD, Stylianakis MM, Stratakis E, Kymakis E. Organic bulk heterojunction photovoltaic devices with surfactant-free Au nanoparticles embedded in the active layer. Appl Phys Lett 2012;100. https://doi.org/10.1063/1.4720510.
[55] Liu X, Wen W, Bazan GC. Post-deposition treatment of an arylated-carbazole conjugated polymer for solar cell fabrication. Adv Mater 2012;24:4505–10. https://doi.org/10.1002/adma.201201567.
[56] Zhou H, Zhang Y, Seifter J, Collins SD, Luo C, Bazan GC, et al. High-efficiency polymer solar cells enhanced by solvent treatment. Adv Mater 2013;25:1646–52. https://doi.org/10.1002/adma.201204306.
[57] Kumar P, Kannappan S, Ochiai S, Shin P-K. High-performance organic solar cells based on a low-bandgap poly-thienothiophene-benzodithiophene polymer and fullerene composite prepared by using the airbrush spray-coating technique. J Kor Phys Soc 2013;62:1169–75. https://doi.org/10.3938/jkps.62.1169.